Engineering a Spin-Orbital Magnetic Insulator by Tailoring Superlattices

J. Matsuno,[1,*,†] K. Ihara,[2] S. Yamamura,[3] H. Wadati,[3,4] K. Ishii,[5] V. V. Shankar,[6] Hae-Young Kee,[6,7] and H. Takagi[1,8,*,‡]

[1]RIKEN Advanced Science Institute, Wako, Saitama 351-0198, Japan
[2]Department of Advanced Materials Science, University of Tokyo, Kashiwa, Chiba 277-8561, Japan
[3]Department of Applied Physics and Quantum-Phase Electronics Center (QPEC), University of Tokyo, Hongo, Tokyo 113-8656, Japan
[4]Institute for Solid State Physics, University of Tokyo, Kashiwa, Chiba 277-8581, Japan
[5]SPring-8, Japan Atomic Energy Agency, Sayo, Hyogo 679-5148, Japan
[6]Department of Physics, University of Toronto, Toronto, Ontario M5S 1A7, Canada
[7]Canadian Institute for Advanced Research, Toronto, Ontario M5G 1Z8, Canada
[8]Department of Physics, University of Tokyo, Hongo, Tokyo 113-0033, Japan

(Received 23 February 2015; published 18 June 2015)

In $5d$ Ir oxides with an interplay of spin-orbit coupling and electron correlations, we have tailored a spin-orbital magnetic insulator out of a semimetal $SrIrO_3$ by tuning the structure through superlattices $[(SrIrO_3)_m, SrTiO_3]$ ($m = 1, 2, 3, 4$, and ∞). We observed the systematic decrease of the magnetic ordering temperature and the resistivity as a function of m. The transition from the semimetal to the insulator is found to be closely linked to the appearance of magnetism at $m \simeq 3$. Long range magnetic ordering was realized even in the $m = 1$ single layer superlattice, implying that the design and realization of novel electronic phases is feasible at the level of a single atomic layer in complex Ir oxides.

DOI: 10.1103/PhysRevLett.114.247209 PACS numbers: 75.70.Tj, 71.27.+a, 71.30.+h, 75.25.-j

Novel interplay of spin-orbit coupling (SOC) and electron correlations in complex Ir oxides (iridates) recently emerged as a new paradigm for correlated electron physics. It is proposed that these iridates may exhibit intriguing phases such as Kitaev spin liquid [1,2] and topological phases [3–13]. The importance of SOC in correlated systems was first recognized in the layered perovskite Sr_2IrO_4 [14,15]. A spin-orbital Mott insulating state is realized with a modest Coulomb U as a consequence of the formation of half-filled $J_{\mathrm{eff}} = 1/2$ states due to the large SOC. In contrast, its three-dimensional counterpart, orthorhombic perovskite $SrIrO_3$ exhibits a semimetal [16,17], where the protected Dirac line nodes generated by the combination of SOC and lattice symmetry make the system topologically robust [7,13]. The transition from such semimetal to magnetic insulator is reported in Ruddlesden-Popper series $Sr_{n+1}Ir_nO_{3n+1}$ ($n = 1, 2$, and ∞), suggesting a dimensionality controlled bandwidth via n [18].

Despite such progress, the microscopic mechanism behind the semimetal-insulator transition, in particular the role of the magnetism, is an open question. It is important to note that $Sr_3Ir_2O_7 (n = 2)$ exhibits a higher magnetic ordering temperature (285 K) [19] than that of Sr_2IrO_4 ($n = 1$, 240 K) [15,20,21] even with a smaller optical gap [18], indicating that the bandwidth change does not account for the magnetism. Furthermore there is a clear sign of anomaly in the resistivity at the magnetic ordering temperature in $n = 2$ [19] whereas such an anomaly is absent in $n = 1$ [21]. To understand how magnetism triggers semimetallic $SrIrO_3$ ($n = \infty$) to magnetic insulator Sr_2IrO_4 ($n = 1$), systematic studies on a series of bulk samples for different n are required. However, bulk $Sr_{n+1}Ir_nO_{3n+1}$ samples for $n \geq 3$ are unstable in ambient pressure and thus difficult to grow.

In this Letter, we report transport and magnetic behaviors of synthesized artificial superlattice $[(SrIrO_3)_m, SrTiO_3]$ with $m = 1, 2, 3, 4$, and ∞. We tracked the evolution of electronic ground states by varying m to understand intimate links among semimetal-insulator transition, magnetism, and underlying lattice structures. Atomically thin slices of $SrIrO_3$, with a number of stacking layers m, were created by inserting insulating $SrTiO_3$ (d^0) layers as illustrated in Fig. 1(a). We found that the magnetic ordering temperature T_c monotonically decreases as a function of m, reaching zero at around $m = 3$. Simultaneously, we observed the transition from insulator to semimetal; in the insulating samples ($m = 1, 2$), the transport shows an anomaly at T_c, suggesting a close relation between charge gap and magnetic ordering. This study reveals how the SOC, correlation, and structures are intertwined together and uncovers that the semimetal-insulator transition is closely linked to the magnetism.

The superlattice samples were fabricated on $SrTiO_3(001)$ substrates by a pulsed laser deposition (PLD) technique using KrF excimer laser pulses focused on a $SrIrO_3$ ceramic target and a $SrTiO_3$ single crystal target. Laser fluence and repetition were 1–2 J/cm^2 and 2 Hz, respectively. The typical substrate temperature was 620 °C and the oxygen pressure was 25 Pa. The repetition of the superlattice, k, is designed so as to make the total thickness about 80 perovskite unit cells. Resonant magnetic x-ray diffraction experiments were performed at beam line 3A at Photon Factory, KEK. Photon polarization of the σ-π'

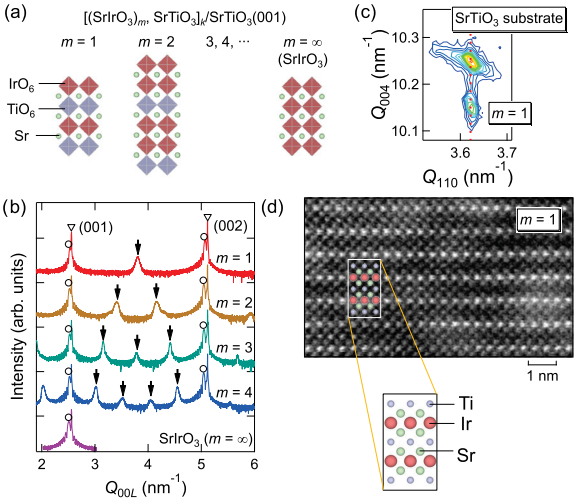

FIG. 1 (color online). (a) Schematics of the superlattices $[(SrIrO_3)_m, SrTiO_3]_k/SrTiO_3(001)$ ($m = 1, 2$, and ∞). (b) X-ray diffraction scans (θ–2θ) of the superlattices ($m = 1, 2, 3, 4$, and ∞). Down arrows indicate the superlattice peaks, while open circles represent the fundamental peaks. Open triangles depict peaks from the substrate. (c) Reciprocal-space mapping of the (114) x-ray diffraction peaks for the superlattice with $m = 1$. (d) Atomically resolved HAADF-STEM image of the superlattice with $m = 1$ along the $SrTiO_3$[100] direction. The schematic of the crystal structure is superposed on the image to show that the brightest spot (Ir) is atomically aligned in the (001) plane.

channel was selectively measured by using a Mo(400) analyzer crystal.

Structural analysis by x-ray diffraction (XRD) clearly demonstrates that the superlattices were fabricated by PLD as designed. Figure 1(b) shows the XRD scans (θ–2θ) of all the samples. In addition to the fundamental peaks originating from the cubic perovskite lattice ($a \sim 0.39$ nm), clear superlattice peaks corresponding to a periodicity of $(m + 1)a$ were observed for all of the superlattices. The in-plane lattice constants of the superlattices are locked to that of the $SrTiO_3$ substrate 0.3905 nm as shown in Fig. 1(c), evidencing the coherent epitaxial growth. The locked lattice constant is much shorter than twice the in-plane Ir-O bond length of Sr_2IrO_4 (0.198 nm) [20], and therefore indicates that the IrO_6 octahedra are rotated around the c axis to accommodate the long Ir-O bonds as in Sr_2IrO_4. An atomically resolved HAADF (high-angle-angular-dark-field)-STEM (scanning transmission electron microscopy) image, with enhanced atomic number contrast, is shown in Fig. 1(d). Ir atoms indicated by the brightest spots are atomically aligned in the [001] plane, demonstrating that atomic order between Ir and Ti is achieved in the coherently grown superlattices.

Upon reducing the number of IrO_2 layers m, the semimetal $SrIrO_3$ perovskite turns into an insulator. For the pure $SrIrO_3$ film ($m = \infty$), metallic behavior of the resistivity $\rho(T)$, though weak, is observed as shown in Fig. 2(a). The large and strongly temperature-dependent

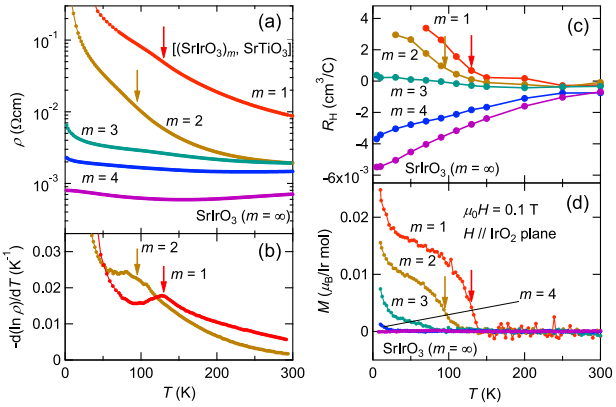

FIG. 2 (color online). Temperature (T) dependence of (a) resistivity (ρ), (b) $-d(\ln\rho)/dT$, (c) Hall coefficient (R_H), and (d) in-plane magnetization (M) for the superlattices ($m = 1, 2, 3, 4$, and ∞). Arrows in each panel indicate the temperatures of the anomaly (T_c) in the resistivity for $m = 2$ and $m = 1$, defined as the peak in $-d(\ln\rho)/dT$.

Hall effect seen in Fig. 2(c) is consistent with the semimetallic ground state of $SrIrO_3$, which was discussed to be a consequence of the presence of Dirac-like nodes [7]. With inserting $SrTiO_3$, $\rho(T)$ systematically changes from metallic to insulating with decreasing the number of adjacent $SrIrO_3$ layers. The $m = 4$ sample appears to be still semimetallic. $m = 3$ is right at the border between metal and insulator, and $m = 2$ and $m = 1$ films appear to be insulating. In the temperature dependence of $\rho(T)$ for $m = 2$ and $m = 1$, anomalies are seen at around $T_c =$ 95 K and 130 K, respectively. The anomalies can be emphasized by taking the derivative $-d(\ln\rho)/dT$, where we observe cusplike peaks as shown in Fig. 2(b). The presence of a cusp means a very rapid increase of resistivity at around T_c on cooling, implying a transition to a strongly insulating state. In accord with this, we see a rapid increase of the Hall coefficient below T_c [22] (For the method of the Hall effect measurements, refer to the Supplemental Material (b) [23]).

The magnetization measurement of these films clearly points to the conclusion that the semimetal-insulator transition is closely linked to the magnetic ordering. Figure 2(d), where the in-plane magnetization $M(T)$ measured at 0.1 T is demonstrated, establishes the link. We observe an in-plane weak ferromagnetism at low temperatures for the films with $m \leq 3$ where an insulating ground state is realized. The magnetization appears to show up around ~100 K and ~140 K for $m = 2$ and $m = 1$. The onset temperatures for weak ferromagnetism agree reasonably well with the temperatures for the anomaly in the resistivity and the Hall effect. The close correlations between the magnetism and transport properties indicate that the magnetism, rather than disorder, is a key ingredient for the semimetal to insulator transition. We note the relatively high resistivity $> 10^{-2}$ Ωcm and the semiconducting temperature dependence for $m = 1$ even above the

magnetic transition (see Supplemental Material (a) for details [23]). This suggests that the Mott character, as in the bulk Sr_2IrO_4, develops in the smallest number of IrO_2 layers, $m = 1$. Later we will discuss the point in terms of first-principles calculation.

In the single layer perovskite Sr_2IrO_4 [15], a weak in-plane magnetic moment emerges in the antiferromagnetically ordered state by canting of the $J_{\text{eff}} = 1/2$ moment, which is produced by the Dzyaloshinskii-Moriya (DM) interaction as a consequence of the rotation of IrO_6 octahedra and the resultant bending of the Ir-O-Ir bond [see Fig. 4(c)]. It is natural to consider that a similar canted in-plane antiferromagnetism is realized in the thin films. The weak ferromagnetic moment in the superlattice was indeed observed only for magnetic field parallel to the IrO_2 plane as indicated in Fig. 3(a), which is consistent with the idea that weak moments originate from the DM interaction associated with the in-plane rotation of IrO_6 octahedra. The resonant magnetic x-ray diffraction at Ir L_3 edge was measured for the $m = 1$ sample with σ-π' polarization to extract the magnetic contribution. The (0.5, 0.5, 5) peak was clearly observed as shown in Fig. 3(b), which confirms the in-plane antiferromagnetic ordering. From these results, we conclude that an in-plane canted antiferromagnetism is realized in the $m = 1$ superlattice. It should be emphasized that the observed long range magnetic ordering in the $m = 1$ sample manifests that we can design and realize novel electronic phases in the unit of the $SrIrO_3$ monolayer.

The canted moment observed for the $m = 1$ superlattice was 0.02 μ_B/Ir mol. This is ~1/4 of the 0.075 μ_B/Ir mol value in the bulk analogue Sr_2IrO_4 [15,21], which implies the reduction of the local Ir moment and/or the reduction of DM interaction. The in-plane lattice constant $a =$ 0.3905 nm for the $m = 1$ sample [see Fig. 1(c)] is larger than the 0.3890 nm value for Sr_2IrO_4 [15] and therefore a smaller rotation of the IrO_6 octahedra is expected for the superlattice. We estimated a rotation angle of approximately 8° in the superlattice from the comparison with the 11°–12° seen in bulk Sr_2IrO_4 [20]. The Ir-O-Ir bond being closer to 180° in the superstructure should decrease the strength of the DM interaction and should increase the bandwidth. The latter makes the system more itinerant and reduces the magnitude of the magnetic moments. In accordance with the expected increase of the bandwidth and itinerancy in the superlattice, the resistivity of the $m = 1$ film is much smaller in magnitude than that of bulk Sr_2IrO_4. We therefore argue that the reduced distortion of the lattice is responsible for the reduced canted moments in the superlattice.

In bulk Sr_2IrO_4, the weak ferromagnetic moment produced by canting is coupled antiferromagnetically along the c axis and the net moment can be observed only above a metamagnetic critical field $H_c = 0.2$ T [15,20,21]. The magnetization curve of the $m = 1$ film with clear hysteresis centered at $H = 0$, shown in Fig. 3(c), shows that the ground state is ferromagnetic rather than antiferromagnetic, implying that the interlayer coupling of canted moments is ferromagnetic, in marked contrast to the case for bulk Sr_2IrO_4. The interlayer coupling of Ir local moments, instead of canted moments, is ferromagnetic since magnetic diffraction with the integer c-axis index$[= (0.5, 0.5, 5)]$ was observed. This is naturally expected because the interlayer coupling of Ir moments through the hybridization with the inserted $SrTiO_3$ layer should give rise to a ferromagnetic Ir-Ir coupling regardless of whether the Ir-Ti coupling is ferromagnetic or antiferromagnetic. To reconcile ferromagnetic coupling of both canted moments and Ir moments, the IrO_6 octahedra in the two adjacent IrO_2 layers should rotate in the same direction, which leads to a magnetic and lattice ordering pattern as schematically illustrated in Fig. 4(a) (see Supplemental Material (c) for more detailed description about magnetic x-ray diffraction [23]).

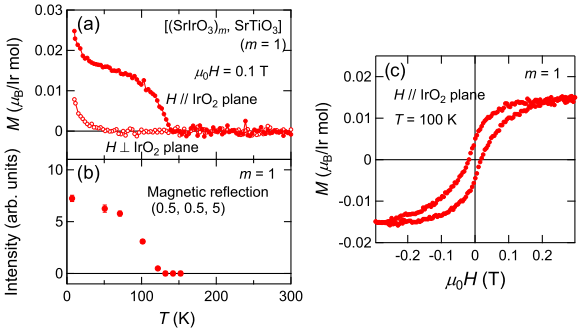

FIG. 3 (color online). (a) Temperature (T) dependence of the magnetization (M) measured at 0.1 T for the superlattice with $m = 1$. The upturn below 50 K, observed for both magnetic field directions, is derived from magnetic impurities in the substrates. (b) Temperature dependence of the magnetic x-ray diffraction intensity for the (0.5, 0.5, 5) peak. The unit cell dimensions are $a \times a \times 2a$ ($a \sim 0.39$ nm). (c) Field dependence of the in-plane magnetization measured at 100 K.

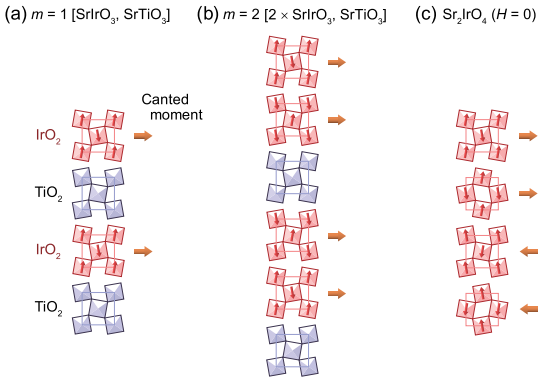

FIG. 4 (color online). Magnetic structures of the superlattices with (a) $m = 1$, (b) $m = 2$, and (c) Sr_2IrO_4 [15]. The phase relation of the IrO_6 rotation between adjacent IrO_2 layers is determined so as to account for the observed magnetic moments [29].

The above argument can be extended to the case for $m = 2$ bilayer, where a weakly ferromagnetic ground state was observed as in the $m = 1$ case. Because of the dominant superexchange process via close to 180° oxygen bonds, the interlayer magnetic coupling within the bilayer unit should be antiferromagnetic [1]. To have a finite canted moment in the bilayer unit, the above interlayer antiferromagnetic coupling requires out-of-phase rotation of IrO_6 octahedra between the two adjacent IrO_2 layers [see Fig. 4(b)] [30–33]. This discussion on the canted in-plane antiferromagnetism can be applied to any number of layers m. The magnetic interactions within the m-IrO_2 blocks should be antiferromagnetic both for the in-plane and the out-of-plane directions, while the coupling between the m-IrO_2 blocks is ferromagnetic. The alternate rotation of IrO_6 octahedra within m-IrO_2 blocks along the stacking direction is always very likely. As long as the orientation of Ir moments is confined within the layers, weak ferromagnetism always shows up and serves as a marker for magnetism and local lattice distortion.

We performed first-principles calculations using density functional theory for $m = 1$ and $m = 2$ superlattices (See Supplemental Material (d) [23] for details of method). We assumed an IrO_6 rotation angle of approximately 8°, which is an estimate from the lattice constant as discussed above. In Figs. 5(a) and 5(b), the band structures of $m = 1$ and $m = 2$ superlattices with small $U = 1$ eV and SOC are shown, respectively. The states near the Fermi level are Ir t_{2g} states with $J_{\mathrm{eff}} = 1/2$ character, the main players in Ir physics. The unoccupied states above ~1 eV are Ir e_g and Ti t_{2g} bands, implying that the $SrTiO_3$ layer indeed acts as an insulating barrier (See Supplemental Material (e) [23] for experimental verification).

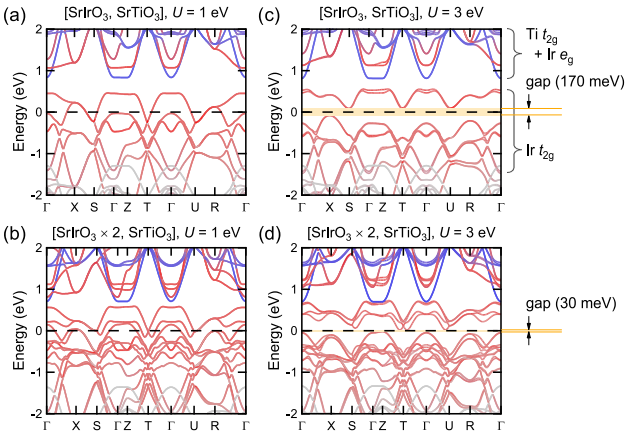

FIG. 5 (color online). Calculated band structures for (a) $m = 1$ and (b) $m = 2$ with $U = 1$ eV. The red and blue colors represent Ir and Ti d-orbitals, respectively. The grey lines dominant below −1.5 eV indicate oxygen p orbitals. The dashed line denotes the Fermi level, and the bands near the Fermi level are mostly of $J_{\mathrm{eff}} = 1/2$ character except near the Γ and Z points. Band structures in the presence of magnetic order for (c) $m = 1$ and (d) $m = 2$ with $U = 3$ eV. Both manifest a charge gap shaded in orange.

For $m = 1$, the $J_{\mathrm{eff}} = 1/2$ bands around the Fermi level are narrow and simple. A half-filled character can be recognized, though marginally. Note that there are degenerated bands along X-S and U-R, cutting across the Fermi level in the middle of the Brillouin-zone lines and hence making a large Fermi surface metal. Since the degeneracy is due to the 90°-rotational symmetry, the system should be metal according to the band theory. Thus electronic correlation could be responsible for a charge gap. With increasing m to 2, the interlayer interaction increases and doubles the number of $J_{\mathrm{eff}} = 1/2$ bands, and a gap opening can be seen at every k point, but due to the presence of small electron and hole Fermi pockets, it becomes a semimetal. We expect that such a semimetallic tendency persists for larger m including $m = \infty$ of $SrIrO_3$ [7]. With the introduction of a reasonably large $U = 3$ eV shown in Figs. 5(c) and 5(d), the evolution from the semimetal ($m = 2$) to the half-filled metal ($m = 1$) changes to the one from a weak to strong magnetic insulator, respectively. A relatively large gap is produced for the case of $m = 1$. In contrast, for $m = 2$, an existing direct gap at all k points for weaker U grows, and a small gap across the Fermi level is then achieved. Since $m = \infty$ is semimetallic with a topologically protected line of node [13], these results account for the experimentally observed evolution from a semimetal to an insulator which is closely linked to a magnetism in $[(SrIrO_3)_m, SrTiO_3]$ superlattices. However, we note significant Mott physics in $m = 1$, as the transport above T_c and the large Fermi surface in the absence of magnetic ordering shown in Fig. 5(a) are not compatible, indicating the importance of correlation in addition to the magnetic ordering.

In conclusion, we have experimentally realized atomically thin slices of perovskite $SrIrO_3$ by inserting monolayers of insulating $SrTiO_3$; $[(SrIrO_3)_m, SrTiO_3]$ ($m = 1, 2, 3, 4$, and ∞) superlattices. With the delicate interplay of strong SOC, electron correlations, and structure, a semimetal-magnetic insulator transition was observed at $m \simeq 3$. Even in the superlattice with only monolayers of $SrIrO_3$ ($m = 1$), we observed long range magnetic ordering, indicating how finely the electronic states are tuned without introducing disorder. Likely due to the relatively weak correlations, the electronic state can be predicted well by first-principles calculations on a quantitative level, which implies that we may tailor a variety of exotic states in the novel family of complex $5d$ transition metal oxides by fabricating superstructures. Based on this success, designing different layer structures of iridates is an interesting future issue, as topological phases are proposed in transition metal oxides with strong SOC [6,7].

This work was supported by a Grant-in-Aid for Scientific Research (No. 24224010 and 25103724) from MEXT, Japan. We would like to thank Y. Yamasaki, H. Nakao, and

Y. Murakami for helpful experimental support at Photon Factory, KEK. Hard x-ray diffraction measurements were performed under the approval of the Photon Factory Program Advisory Committee (Proposal No. 2011G062) at the Institute of Material Structure Science, KEK. V. V. S. and H. Y. K. are supported by NSERC of Canada. Computations were performed on GPC supercomputer at the SciNet HPC Consortium. SciNet is funded by: the Canada Foundation for Innovation under the auspices of Compute Canada; the Government of Ontario; Ontario Research Fund—Research Excellence; and the University of Toronto.

*To whom all correspondence should be addressed.
†Present address: RIKEN Center for Emergent Matter Science (CEMS), Wako, Saitama 351-0198, Japan.
matsuno@riken.jp
‡takagi@phys.s.u-tokyo.ac.jp

[1] G. Jackeli and G. Khaliullin, Phys. Rev. Lett. **102**, 017205 (2009).
[2] W. Witczak-Krempa, G. Chen, Y.-B. Kim, and L. Balents, Annu. Rev. Condens. Matter Phys. **5**, 57 (2014).
[3] A. Shitade, H. Katsura, J. Kuneš, X.-L. Qi, S.-C. Zhang, and N. Nagaosa, Phys. Rev. Lett. **102**, 256403 (2009).
[4] D. Pesin and L. Balents, Nat. Phys. **6**, 376 (2010).
[5] B.-J. Yang and Y. B. Kim, Phys. Rev. B **82**, 085111 (2010).
[6] D. Xiao, W. Zhu, Y. Ran, N. Nagaosa, and S. Okamoto, Nat. Commun. **2**, 596 (2011).
[7] J.-M. Carter, V. V. Shankar, M. A. Zeb, and H.-Y. Kee, Phys. Rev. B **85**, 115105 (2012).
[8] Y.-Z. You, I. Kimchi, and A. Vishwanath, Phys. Rev. B **86**, 085145 (2012).
[9] E.-G. Moon, C. Xu, Y. B. Kim, and L. Balents, Phys. Rev. Lett. **111**, 206401 (2013).
[10] Z. Y. Meng, Y.-B. Kim, and H.-Y. Kee, Phys. Rev. Lett. **113**, 177003 (2014).
[11] B. J. Yang and N. Nagaosa, Phys. Rev. Lett. **112**, 246402 (2014).
[12] Y. Chen and H.-Y. Kee, Phys. Rev. B **90**, 195145 (2014).
[13] Y. Chen, Y.-M. Lu, and H.-Y. Kee, Nat. Commun. **6**, 6593 (2015).
[14] B. J. Kim, H. Jin, S. J. Moon, J.-Y. Kim, B.-G. Park, C. S. Leem, J. Yu, T. W. Noh, C. Kim, S.-J. Oh, J.-H. Park, V. Durairaj, G. Cao, and E. Rotenberg, Phys. Rev. Lett. **101**, 076402 (2008).
[15] B. J. Kim, H. Ohsumi, T. Komesu, S. Sakai, T. Morita, H. Takagi, and T. Arima, Science **323**, 1329 (2009).
[16] S. Y. Jang, H. Kim, S. J. Moon, W. S. Choi, B. C. Jeon, J. Yu, and T. W. Noh, J. Phys. Condens. Matter **22**, 485602 (2010).
[17] Y. F. Nie, P. D. C. King, C. H. Kim, M. Uchida, H. I. Wei, B. D. Faeth, J. P. Ruf, J. P. C. Ruff, L. Xie, X. Pan, C. J. Fennie, D. G. Schlom, and K. M. Shen, Phys. Rev. Lett. **114**, 016401 (2015).
[18] S. J. Moon, H. Jin, K. W. Kim, W. S. Choi, Y. S. Lee, J. Yu, G. Cao, A. Sumi, H. Funakubo, C. Bernhard, and T. W. Noh, Phys. Rev. Lett. **101**, 226402 (2008).
[19] G. Cao, Y. Xin, C. S. Alexander, J. E. Crow, P. Schlottmann, M. K. Crawford, R. L. Harlow, and W. Marshall, Phys. Rev. B **66**, 214412 (2002).
[20] M. K. Crawford, M. A. Subramanian, R. L. Harlow, J. A. Fernandez-Baca, Z. R. Wang, and D. C. Johnston, Phys. Rev. B **49**, 9198 (1994).
[21] G. Cao, J. Bolivar, S. McCall, J. E. Crow, and R. P. Guertin, Phys. Rev. B **57**, R11039 (1998).
[22] We did not observe any nonlinearity nor hysteresis in Hall resistivity as a function of the magnetic field up to 9 T in all of the samples. The latter indicates the absence of the anomalous Hall effect, which is consistent with the in-plane magnetization shown in Fig. 3(a).
[23] See Supplemental Material at http://link.aps.org/supplemental/10.1103/PhysRevLett.114.247209 for details of the method, which includes Refs. [24–28].
[24] The Elk FP-LAPW Code (2013), http://elk.sourceforge.net.
[25] D. M. Ceperley and B. J. Alder, Phys. Rev. Lett. **45**, 566 (1980).
[26] J. P. Perdew and A. Zunger, Phys. Rev. B **23**, 5048 (1981).
[27] M. T. Czyżyk and G. A. Sawatzky, Phys. Rev. B **49**, 14211 (1994).
[28] K. Kobayashi, Nucl. Instrum. Methods A **601**, 32 (2009).
[29] While we have no experimental information on TiO_6 rotation, we assumed it to be out of phase with the neighboring IrO_6 rotation since it is reasonable to avoid Coulomb repulsion between oxygen atoms.
[30] In bulk bilayer $Sr_3Ir_2O_7$ ($n = 2$), the Ir moments are found to form a collinear antiferromagnetic alignment along the c axis [31,32], in marked contrast to the $m = 2$ film. Theoretically, the two states with the canted in-plane antiferromagnetism and the collinear out-of-plane antiferromagnetism are energetically almost degenerate for $Sr_3Ir_2O_7$ [33], which may account for the contrasting behavior of the $m = 2$ film and $Sr_3Ir_2O_7$.
[31] J. W. Kim, Y. Choi, J. Kim, J. F. Mitchell, G. Jackeli, M. Daghofer, J. van den Brink, G. Khaliullin, and B. J. Kim, Phys. Rev. Lett. **109**, 037204 (2012).
[32] S. Fujiyama, K. Ohashi, H. Ohsumi, K. Sugimoto, T. Takayama, T. Komesu, M. Takata, T. Arima, and H. Takagi, Phys. Rev. B **86**, 174414 (2012).
[33] J.-M. Carter and H.-Y. Kee, Phys. Rev. B **87**, 014433 (2013).